A High-Accuracy Rainfall Dataset by Merging Multi-Satellites and Dense Gauges over Southern Tibetan Plateau for 2014-2019 Warm Seasons

Kunbiao Li[1], Fuqiang Tian[1], Mohd Yawar Ali Khan[2], Ran Xu[1], Zhihua He[3], Long Yang[4], Hui Lu[5], Yingzhao Ma[6]

[1] Department of Hydraulic Engineering, Tsinghua University, Beijing, China

[2] Department of Hydrogeology, King Abdul-Aziz University, Jeddah, Saudi Arabia

[3] Centre for Hydrology, University of Saskatchewan, Saskatoon, SK S7N 5C8, Canada

[4] School of Geography and Ocean Science, Nanjing University, Nanjing, China

[5] Department of Earth System Science, Tsinghua University, Beijing, China

[6] Cooperative Institute for Research in the Atmosphere, Colorado State University, 1375 Campus Delivery, Fort Collins, CO 80523, United States.

Correspondence: Fuqiang Tian (tianfq@mail.tsinghua.edu.cn)

Abstract

Tibetan Plateau (TP) is well known as the Asia's water tower from where many large rivers originate. However, due to complex spatial variability of climate and topography, there is still a lack of high-quality rainfall dataset for hydrological modelling and flood prediction. This study, therefore, aims to establish a high-accuracy daily rainfall product through merging rainfall estimates from three satellites, i.e., GPM-IMERG, GSMaP, and CMORPH, based on the likelihood measurements of a high-density rainfall gauge network. The new merged daily rainfall dataset with a spatial resolution of 0.1°, focuses on warm seasons (June 10th - October 31st) from 2014 to 2019. Statistical evaluation indicated that the new dataset outperforms the raw satellite estimates, especially in terms of rainfall accumulation and the detection of ground-based rainfall events. Hydrological evaluation in the Yarlung Zangbo River Basin demonstrated high performance of the merged rainfall dataset in providing accurate and robust forcings for streamflow simulations. The new rainfall dataset additionally shows superiority to several other products of similar types, including MSWEP and CHIRPS. This new rainfall dataset is publicly accessible at https://doi.org/10.11888/Hydro.tpdc.271303 (Li et al.,2021).

1. Introduction

Precipitation, linking atmospheric and hydrological processes, serves as a crucial component of the water cycle (Eltahir & Bras, 1996; Trenberth et al., 2003). Gridded precipitation datasets become more and more popular with the advent of satellite precipitation measurement. Most famous satellite gridded precipitation datasets include Tropical Rainfall Measuring Mission (TRMM) (Huffman et al., 2007) and its successor the Integrated Multi-satellite Retrievals for Global Precipitation Measurement mission (GPM-IMERG) (Hou et al., 2014), the Global Satellite Mapping of Precipitation

(GSMaP) (Ushio et al., 2009), the Climate Prediction Centre (CPC) MORPHing technique (CMORPH) (Joyce et al., 2004), etc. These products have been successfully applied in various hydrometeorological studies and water resources management practices (Kidd, C., & Levizzani, V., 2011; Jiang et al., 2012; Tong et al., 2014; Yang et al., 2015; Sun et al., 2016; Wang et al., 2017).

However, all existing precipitation datasets show insufficient accuracy in high mountainous regions (Yilmaz et al., 2016; Derin et al., 2018; Derin et al., 2019; Anagnostou & Zhang, 2019), which hinders our understanding of climate and hydrological processes over these areas. This can be attributed to the complex physical nature of electromagnetic transmission and precipitation forming processes (Hong et al., 2007; Bitew & Gebremichael 2010; Dinku et al., 2010), and harsh environments in high mountains that lead to very limited deployment of in-situ rain gauges with insufficient representation of ground observations for training satellite-based precipitation retrieval algorithms. For instance, the Tibetan Plateau (TP) as the roof of the world is surrounded by imposing mountain ranges with an average elevation exceeding 4000 m. It generates several large rivers in Asia and provides invaluable freshwater resources for more than 1.4 billion people living downstream (Immerzeel et al., 2010). However, this vast plateau has very limited number of precipitation gauges across its 2.5 million km^2 area. The precipitation gauge network operated by China Meteorological Agency (CMA) contains only 86 gauges over the entire TP (Figure 1). These gauges are essential to correct satellite precipitation datasets. For example, GPM-IMERG 'Final' Run dataset uses Global Precipitation Climatology Centre (GPCC) database, GSMap_Gauge and CMORPH use NOAA Climate Prediction Centre (CPC) database. Although both GPCC and CPC databases received data through Global Telecommunication System (GTS), only part of the above-mentioned gauges in TP were utilized (Xie et al., 2007; Becker 2013). Previous evaluations over the TP indicated that most products present dependence on topography to varying degrees, and products adjusted by gauge observations shows better performance than satellite-only

products (Gao et al.,2013; Lu et al., 2018). Therefore, a better spatial coverage of rain gauges is critical to correct satellite products in high mountains.

In 2014, the Ministry of Water Resources of China (MWR) launched the flash flood monitoring and alarming campaign. A large number of rain gauges is now accessible over the TP, especially in the southern TP. There are 440 new rain gauges totally involved in 6 years, and are available since 2014, independent of the existing CMA precipitation gauge network (Figure 1). These gauges provide measurements of precipitation in liquid phase (i.e., rainfall) at event time scale. A couple of recent studies have demonstrated the utility of this rain gauge network (Xu et al., 2017; He et al., 2017; Tian et al., 2018; Wang et al., 2020). For instance, Xu et al. (2017) evaluated the performance of TRMM and GPM and the dependence on topography and rainfall intensity based on the network. Their results demonstrated that the data quality of this dense gauge network is strictly controlled, serving as the currently highest gauge dense for satellite product evaluation on TP. Wang et al. (2020) used the gauge data to validate their reproduced precipitation dataset. However, there is not a merging product that assimilate the observations from this dense rain gauge network. This is apparently a unique opportunity to improve the performance of existing satellite-based precipitation datasets for its highest density and quality.

This study aims to provide a high-accuracy rainfall dataset by merging all available ground gauges and three good-quality satellite precipitation datasets over the southern TP for the warm seasons (June 10th - October 31st) from 2014 to 2019. The remainder of this paper is organized as follows: Section 2 describes the study area and the source data. Section 3 provides details of the data merging method and the methods adopted to evaluate the quality of dataset. Results are presented in Section 4. The data availability and summary are provided in Section 5 and Section 6, respectively.

2. Study Area and Source Data

2.1. Southern Tibetan Plateau

Tibetan Plateau, known as the Asian water tower, mainly covers parts of China, India, Myanmar, Bhutan, Nepal and Pakistan. Various climate systems affect the plateau, including westerly winds in winter and the Indian monsoon in summer (Yao et al., 2012). Many Asian large rivers originate from this vast area, including the Yellow River, the Yangtze River, the Yarlung Zangbo River (YZR), Jinsha River (JR), Lancang River (LR), Salwen River (SR), Irrawaddy River (IR), Ganges River (GR), and Indus River (IDR). This study is focused on the southern part of TP (Figure 1), including the upper YZR Basin (YZRB) as a major basin.

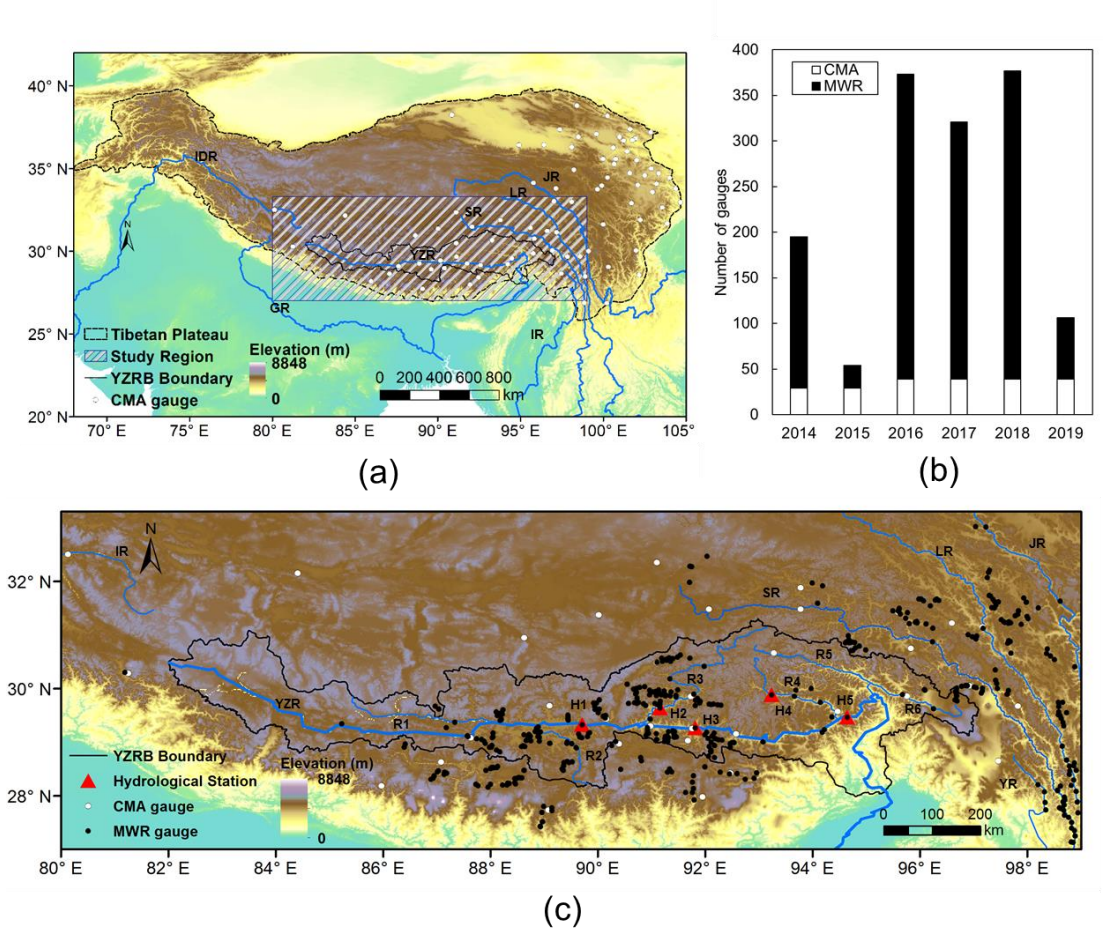

Figure 1. (a) The location and topography of the TP and the spatial distributions of CMA gauges. (b) Numbers of ground gauges installed by CMA and MWR in southern TP during 2014-2019, (c)

Locations of CMA and MWR rain gauges and main hydrological stations in southern TP. The names of hydrological stations are labelled as H1-Yangcun, H2-Lhasa, H3-Nugesha, H4-Gongbujiangda, H5-Nuxia. The names of tributary rivers are labelled as R1-Duoxiong Zangbo, R2-Nianchu River, R3-Lhasa River, R4-Niyang River, R5-Yigong Zangbo, R6-Parlung Zangbo.

2.2. Ground gauged rainfall

We combined two rain gauge networks managed by MWR and CMA to obtain a high-quality ground reference dataset up to date. The number of rain gauge is presented in Figure 1b, and varies across different years. The spatial distribution of all gauges is presented in Figure 1c. The gauges are mainly located in the middle reaches of YZRB and the east part of the study area. Despite the high density, we can see these rain gauges are not evenly distributed across the space. This makes satellite rainfall products over varying altitudes and aspects important. Daily rainfall observations during the warm seasons of 2014-2019 were accumulated from the original event scale measurements. Total number of the CMA and MWR gauges ranges from 53 in 2015 to 377 in 2018, forming the densest rain gauge network up till now.

The CMA gauge data has been widely demonstrated as reliable and accurate in previous studies (Zhai et al., 2005; Su et al., 2020; He et al., 2020). Gauge data used in this study has been manufactured under strict quality control procedures, including (1) internal consistency check, (2) extreme values check (0~85mm/h), and (3) spatial consistency check (Ren et al., 2010). Rain gauges with erroneous values (e.g. enormously large values) were discarded from the entire records. In cold seasons there are many missing values and only few gauges meet the requirements of the strict quality control method. So the warm seasons from June 10th to October 31st were selected as the study period to maintain the high quality of outcome rainfall dataset. While rainfall gauged data is continuously collected to update our merged rainfall data.

2.3. Satellite Precipitation Datasets

Three satellite precipitation products were chosen for the data merging procedure (Lu et al., 2019; Derin et al., 2019; Tang et al., 2020), including GPM-IMERG 'Final' run (here after referred to as IMERG) from the National Aeronautics and Space Administration (NASA) (https://disc.gsfc.nasa.gov/), the GSMaP_Gauge (here after referred to as GSMaP) from Japan Aerospace Exploration Agency (JAXA) (http://sharaku.eorc.jaxa.jp) and the CMORPH v1.0 from NOAA CPC (ftp://ftp.cpc.ncep.noaa.gov/precip/CMORPH_V1.0/). Spatial resolutions and temporal frequency of the satellite datasets are listed in Table 1. To be consistent, IMERG and GSMaP data were accumulated to daily scale (08:00-08:00 of local time, i.e. UTC+8) and CMORPH was bilinearly interpolated to the grid resolution of 0.1°.

The merged dataset was further compared with two popular merged rainfall datasets of Climate Hazards Group InfraRed Precipitation with Stations (CHIRPS) (Funk et al., 2015) and Multi-Source Weighted-Ensemble Precipitation (MSWEP) (Beck et al., 2019). CHIRPS was originated by merging CHPClim, thermal infrared, TRMM3B42, NOAA CFSv2 precipitation data, and ground observation precipitation data. MSWEP was merged from multiple datasets including CPC, GPCC, CMORPH, GSMaP-MVK, GPM-IMERG, ERA5, and JRA-55. CHIRPS and MSWEP showed great potentials in rainfall estimates in previous studies (Liu et al., 2019).

Table 1. Multiple satellite precipitation datasets used in this study.

Datasets	Resolution	Frequency	Source	Reference
GPM IMERG	0.1 °x 0.1 °	0.5 hourly	NASA	(Hou et al., 2014)
GSMaP_Gauge	0.1 °x 0.1 °	1 hourly	JAXA	(Ushio et al., 2009)
CMORPH v1.0	0.25 °x 0.25 °	daily	CPC	(Joyce et al., 2004)
CHIRPS v2.0	0.25 °x 0.25 °	daily	USGS and CHC	(Funk et al., 2015)
MSWEP v2	0.1 °x 0.1 °	3 hourly	-	(Beck et al., 2019)

3. Methodology

We used the Dynamic Bayesian Model Averaging (DBMA) method (Ma et al., 2017) to merge the satellite datasets with in-situ rain gauges. To evaluate the quality of the new dataset, we carried out statistical and hydrological evaluations and comparisons with CHIRPS and MSWEP in southern TP.

3.1. Dynamic Bayesian Model Averaging method

The Dynamic Bayesian Model Averaging (DBMA) method developed by Ma et al. (2018) was utilized in this work. A flow chart of the merging method is shown in Figure 2. In the first step, a training dataset was formed by selecting samples from the ground gauged data and three original satellite datasets. The training period was set as 40 days. Increasing the length of the training period did not lead to obvious improvement of the merging method (Ma et al., 2018). In the second step, the training dataset was transformed by the Box-Cox Gaussian distribution, and the optimal weights for each of the original satellite datasets on a specific grid where a ground gauge is located on each training day were estimated by a logarithmic likelihood equation and the optimal expectation algorithm. In the third step, an ordinary Kriging interpolation method was applied to spatially interpolate the daily weights onto grids with no gauges. Finally, posterior spatiotemporal weights were used to obtain the final merged rainfall dataset. The DBMA-merged data has been proved in Ma et al. (2017) to outperform original satellite data during 2007-2012 over TP.

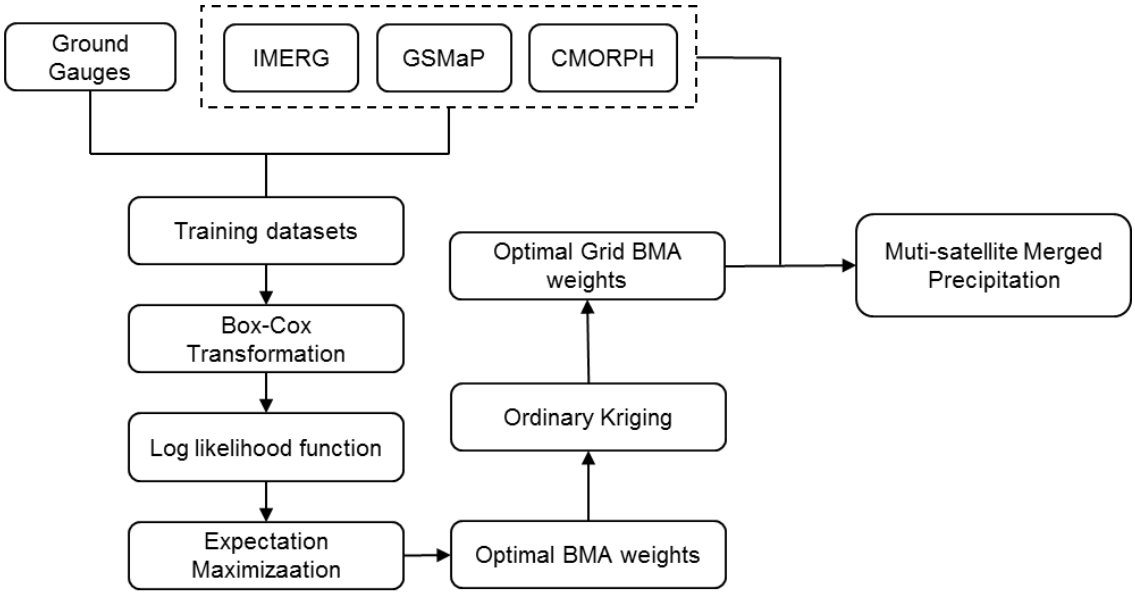

Figure 2. Flowchart of the DBMA merging method (adapted from Ma et al., 2018).

For statistical evaluation of the merged data against ground gauges, around 85% of the gauges were randomly selected to form a training gauge set for the merging approach in each year during 2014-2019, and the remaining 15% were used for test. Training method DBMA of 40 days was only conducted in training dataset. Table 2 lists the numbers of training and test gauges in each of the warm seasons. The spatial distributions of gauges in each year are presented in Figure S1. Data from all gauges were involved in the training procedure of the final released version of the merged data.

Table 2. Number of rain gauges for training and test in 2014-2019.

Year	Total number of rain gauges	Number of training gauges	Number of test gauges
2014	195	166	29
2015	54	46	8
2016	373	317	56
2017	321	273	48
2018	377	320	57
2019	106	90	16

3.2. Statistical Evaluation

Performance of the multiple datasets were statistically evaluated by comparing

185 with ground observations on the corresponding statelite grids. Relative bias (RB) and
186 normalized root mean square error (RMSE) were adopted to measure the amount
187 difference between the gridded rainfall and the gauged rainfall. Correlation Coefficient
188 (CC) was used to evaluate the consistency between satellite estimates and gauge
189 observations. The skill of rainfall data on detecting rainfall occurrence (rainfall events
190 higher than zero) was evaluated through a set of metrics (similarly to Wilks, 2006): i.e.
191 the probability of detection (POD) assessing how good the multiple rainfall datasets are
192 at detecting the occurrence of rainfall, false alarm ratio (FAR) measuring how often the
193 gridded rainfall datasets detect rainfall when there actually is not rainfall, and critical
194 success index (CSI) measuring the ratio of rainfall events that are correctly detected by
195 the gridded datasets to the total number of observed or detected events. Equations for
196 the above metrics are shown in Table 3.

197 Table 3. Statistical indices that were used to assess the performance of the gridded rainfall
198 datasets.

Statistical Indicators	Equation	Optimal Value	Equation number
Relative Bias (RB)	$Bias = \frac{\sum_{i=1}^{n}(S_i - G_i)}{\sum_{i=1}^{n} G_i}$	0	(1)
Correlation Coefficient (CC)	$CC = \frac{[\sum_{i=1}^{n}(S_i - \bar{S}) \cdot (G_i - \bar{G})]^2}{\sum_{i=1}^{n}(S_i - \bar{S})^2 \cdot \sum_{i=1}^{n}(G_i - \bar{G})^2}$	1	(2)
Root Mean Square Error (RMSE)	$RMSE = \sqrt{\frac{1}{n}\sum_{i=1}^{n}(S_i - G_i)^2}$	0	(3)
Probability of Detection (POD)	$POD = \frac{a}{a+c}$	1	(4)
False Alarm Ratio (FAR)	$FAR = \frac{b}{a+b}$	0	(5)
Critical success index (CSI)	$CSI = \frac{a}{a+b+c}$	1	(6)

199 For the equations listed in Table 3, n is the total number of gridded product data
200 and gauge observation data; i is the i^{th} of satellite product data and gauge

observation data; G_i means gauge observation and $\overline{G}$ is the average of gauge observation. S_i and $\overline{S}$ are gridded estimates and their average, respectively. a represents hit (i.e., event was detected to occur and observed to occur), b represents false alarm (i.e., event was detected to occur but not observed to occur), and c represents miss (i.e., event was not detected to occur but observed to occur).

Triple Collocation (TC) technique provides a platform for quantifying the root mean square errors of three products that estimate the same geophysical variable (Stoffelen, 1998). Roebeling et al. (2012) successfully applied the TC technique to estimate errors of three rainfall products across Europe. An extended Triple Collocation (ETC) introduced in Kaighin et al. (2014), which is able to estimate errors and correlation coefficients with respect to an unknown target was used in this study to compare the performance of the DBMA-merged data and two previous merged datasets of CHIRPS and MSWEP.

3.3. Hydrological Evaluation

In addition to the statistical assessments against rain gauges, hydrological assessment was used as a tool to test the performance of merged rainfall datasets on forcing hydrological modelling in the study area (similarly see Yong et al, 2012; Xue et al, 2013; Yong et al, 2014; Li et al, 2014). In this section, a semi-distributed hydrological model developed by Tian (2006), namely Tsinghua Hydrological Model based on Representative Elementary Watershed (THREW), was adopted for the hydrological assessment of rainfall datasets in the YZRB. YZRB has a drainage area of approximately 240,480 km^2 within China's boarder. The basin elevation ranges from 143 to 7,261 m, with an average of around 4,600 m. YZR is one of the most important transboundary rivers in South Asia and the highest river in the world, which is characterized by a dynamic fluvial regime with exceptional physiographic setting spreading along the eastern Himalayan region (Goswami, 1985). Due to complex terrain and strongly varying elevation, the YZRB is under control of a variety of climate

systems, such as the semi-arid plateau climate prevailing in the upper and middle reaches, and the mountainous subtropical and tropical climates prevailing in the lower reaches. In the cold upper reaches, the mean annual rainfall is less than 300 mm. In the warm middle reaches, the mean annual rainfall falls between 300 mm and 600 mm.

The whole basin area above the Nuxia hydrological station was divided into 63 Representative Elementary Watersheds (REWs). Model parameters were calibrated by daily discharges measured at the Nuxia station. The calibration period is scheduled to run in the warm seasons from June 10th to October 31st in 2014- 2017, encompassing a period length of 576 days. The validation period includes two warm seasons in 2018 and 2019 with a total duration of 288 days. Descriptions of the calibrated model parameters can be found in Table 4. An automatic algorithm pySOT developed by D. Eriksson et al (2019) was used to optimize the parameter values based on an objective-function of *NSE* (Nash and Sutcliffe, 1970) in Eq. 7. To conduct a continuous hydrological simulation in the study period, the datasets of daily grid-based precipitation over China (Zhao et al., 2014) were used as model inputs in the non-warm seasons when merged rainfall is not available.

Table 4. Calibrated parameters of the THREW model.

Symbol	Description	Unit	Value Range
kv	Fraction of potential transpiration rate over potential evaporation	-	0.001-0.8
n^t	Manning roughness coefficient for hillslope	-	0.0001-0.2
GaIFL	Spatial heterogeneous coefficient for infiltration capacity	-	0.0001-0.7
GaEFL	Spatial heterogeneous coefficient for exfiltration capacity	-	0.0001-0.7
GaETL	Spatial heterogeneous coefficient for evapotranspiration capacity	-	0.0001-0.7
WM	Tensor water storage capacity	cm	0.1-10
B	Shape coefficient to calculate the saturation excess runoff area	-	0.01-1
Gaus	Coefficient representing spatial heterogeneity of exchange term between t-zone and r-zone	-	0.001-10

KKA	Exponential coefficient to calculate subsurface flow	-	0.01-6
KKD	Linear coefficient to calculate subsurface flow	-	0.001-0.5
MM	Snow melting degree-day factor	mm/day	0.001-10
MMG	Ice melting degree-day factor	mm/day	0.001-10
C1+C2	Muskingum parameter	-	0.0001-1
C1/(C1+C2)	Muskingum parameter	-	0.0001-1

$$NSE = 1 - \frac{\sum_{n=1}^{N}(Q_{obs}^{n} - Q_{sim}^{n})^2}{\sum_{n=1}^{N}(Q_{obs}^{n} - \bar{Q}_{obs})^2} \quad (7)$$

where, N is the total number of days in the evaluation period, Q_{obs}^{n} and Q_{sim}^{n} represent the observed and simulated runoff on the n^{th} day, respectively. $\bar{Q}_{obs}$ represents the average of observed runoff in the evaluation period.

4. Results and Discussions

4.1. Spatiotemporal Patterns

Based on the merging method, a new daily rainfall dataset with spatial resolution of 0.1°×0.1° in the warm seasons from June 10th to October 31st (144 days in each year) in 2014-2019 (864 days in six years) was generated. Figure 3 presents the spatial pattern of the mean rainfall over the six warm seasons of the merged data in southern TP. It is shown that extremely high summer rainfall centres concentrate in the south-eastern and south-western of the study area where is known as a world-famous heavy rainfall centre (see Biskop et al., 2015; Bookhagen & Burbank, 2006; Kumar et al., 2010).

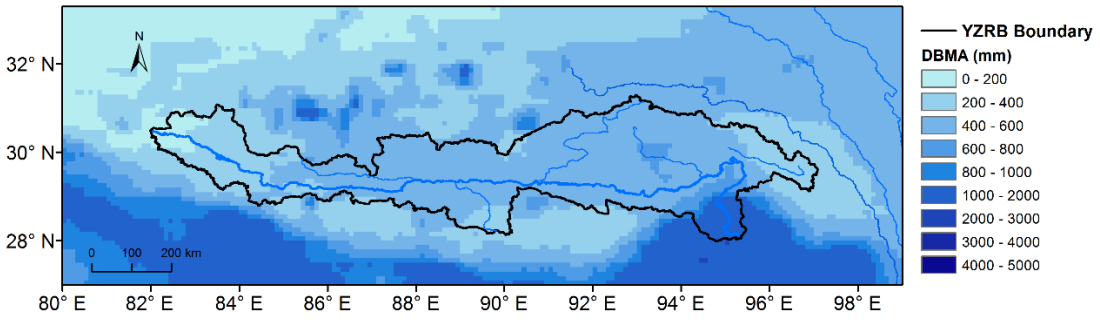

Figure 3. Spatial pattern of mean rainfall over six warm seasons in 2014-2019 of the DBMA-

merged data in southern TP.

In addition, Figure 4 compares the time series of average daily weight and rainfall over the YZRB basin derived from the DBMA-merged data and the original satellite datasets. As expected, the DBMA-merged daily rainfall in general fall in the envelope ranges of the three satellite datasets. Merged data is closer to CMORPH in June, September and October, while showing equal closeness to all the three source satellite data in July and August. It indicates that CMORPH is closer to the in-situ gauges than IMERG at basin scale when rainfall value is small, especially for light rainfall events smaller than 2 mm, but this difference tends to be small for heavy rainfall events.

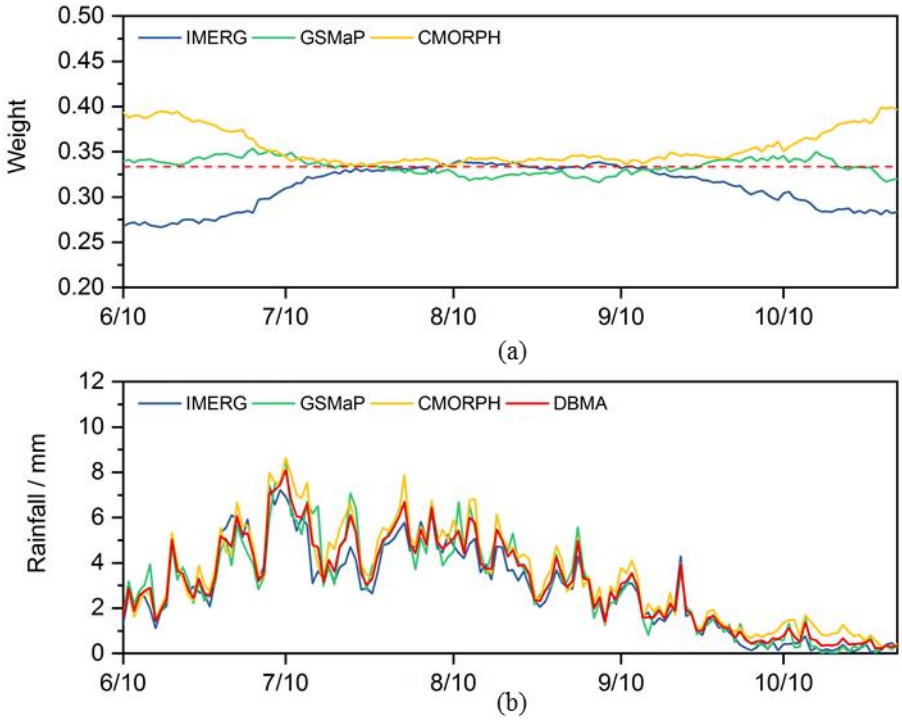

Figure 4. Seasonal variations in basin-averaged (a) weights and (b) rainfall estimates of the multiyear daily values of IMERG, GSMaP, CMORPH and DBMA.

4.2. Statistical Evaluation

Figure 5 shows the statistical evaluation of the merged and original datasets in the warm seasons. The statistical indices were calculated for three gauge groups including the training gauges, the test gauges and all gauges at different elevation bands. The

datasets in general presented comparable performance for the training and test gauge groups, indicating that the sampling procedure of ground gauges is adequately random. The comparable performance of merged data in training and test gauge groups demonstrated robustness of the merging method on varying gauges. In terms of RSME, CC, and POD, the DBMA-merged data shows much better performance on all gauge groups and elevation bands than the original satellite datasets. The smallest RSME of merged data indicate that the total rainfall amount of the merged data during the evaluation period showed the lowest difference from the total amount of gauged rainfall. The highest CC and POD highlight the best consistency between merged data and ground gauge data on days when most regions in the basin were rainy. The RB of DBMA-merged data is at an intermediate level among the satellite datasets as it is the weighted average of those three datasets. The higher FAR and lower CSI of DBMA-merged data could be attributed to that the merging method detected rainfall events when rainfall estimate is higher than zero in any one of the three satellite datasets and thus resulted in overestimated rainfall occurrence. The overestimated rainfall occurrence might have small effects on the estimation of rainfall amount, as most of the falsely alarmed events were tiny. It is noteworthy that the performance of the merged data shows smaller variance across elevation bands than that of the original satellite datasets. This is most likely benefiting from the spatially dynamic optimal weights for the original satellite data. However, the merged data presented the largest difference from gauged data at the altitudes of 3000-3500 m, because there are much less gauges on this elevation zone.

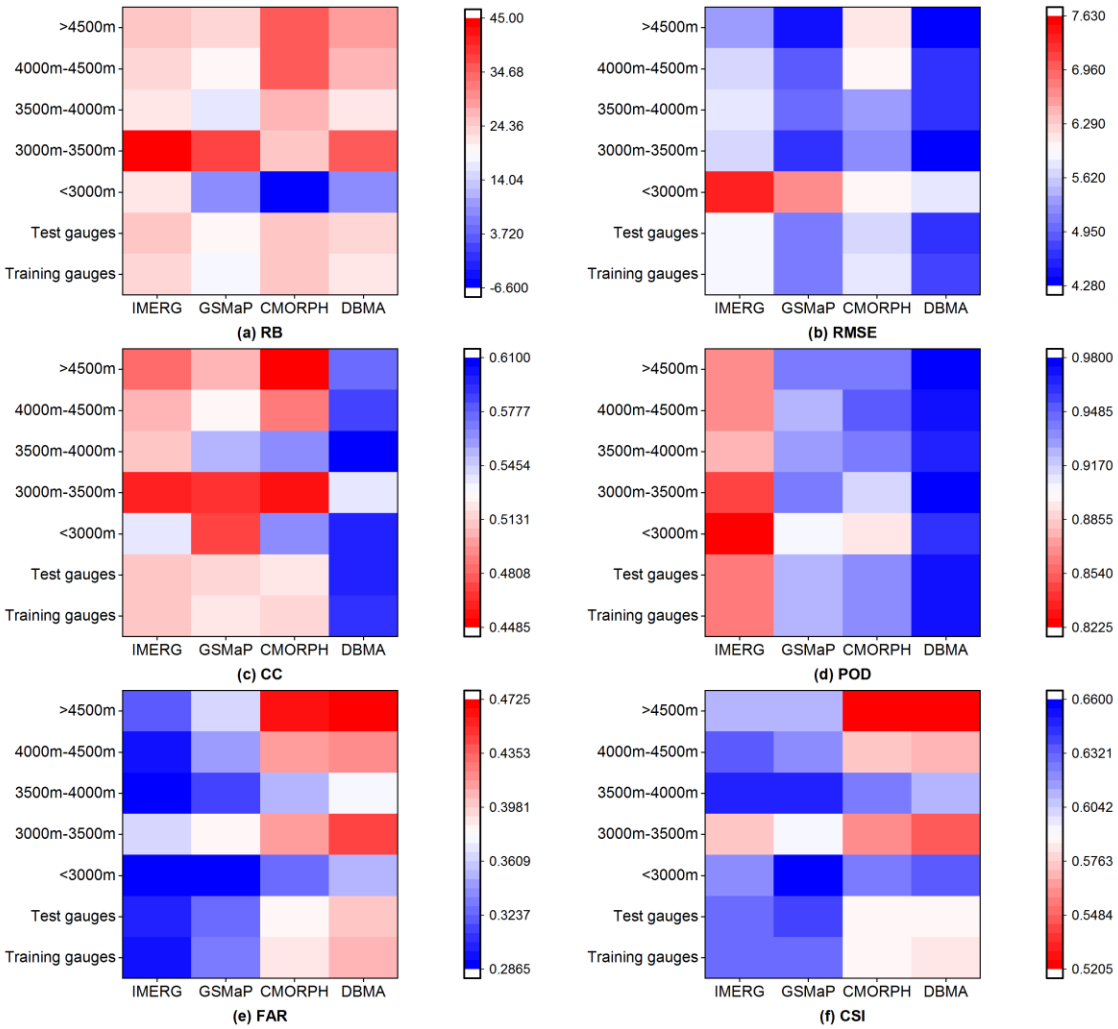

Figure 5. Comparisons of the statistical indices of (a) RB, (b)RMSE, (c) CC, (d) POD, (e) FAR and (f) CSI for training gauges, test gauges and all gauges at five elevation bands.

Figure 6 shows CC of different datasets on specific gauges. The merged data presents higher CC values in regions where are densely gauged, i.e., the middle reaches of YZRB and the east part of the study region, which can be expected as the dense ground gauges provided strongly informative benchmark likelihoods for the estimation of satellite data weights. On most of the gauges (Figure 6a), the merged-data presented higher CC values than the IMERG data, which is consistent with Figure 5c. On contrary, the merged-data showed reduced CC than GSMaP and CMORPH on more gauges (Figures 6b-c), indicating that involving IMERG data in the merging procedure on these gauges lead to deteriorated consistence performance.

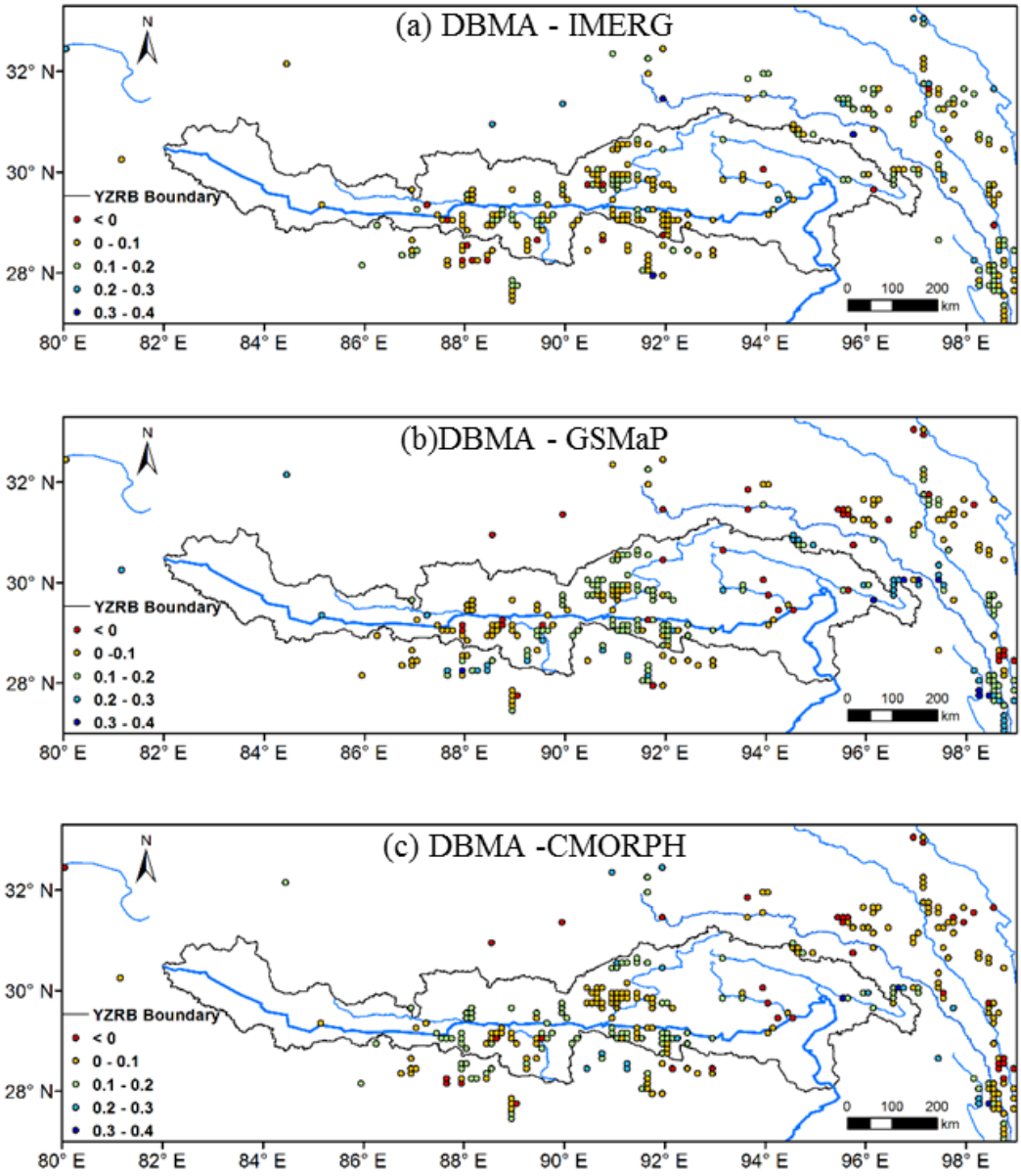

Figure 6. Spatial distributions of CC difference between (a) DBMA and IMERG, (b) DBMA and GSMaP, (c) DBMA and CMORPH

4.3. Hydrological Evaluation

(a) Hydrological simulation

Performance of the THREW model forced by different rainfall datasets are compared in Table 5. The DBMA-merged dataset achieved the best runoff simulation among all rainfall inputs, with NSE reaching 0.93 and 0.86 in calibration and validation period, respectively, indicating an excellent agreement between simulated and observed

hydrographs. Both IMERG and GSMaP underestimated the measured daily discharge, but the DBMA-merged dataset improved such underestimations (see *RB* values in Table 4).

Table 5. Evaluation metrics of hydrological simulations forced by IMERG, GSMaP, CMORPH and DBMA.

Parameters	IMERG	GSMaP	CMORPH	DBMA
NSEcal	0.91	0.90	0.90	0.93
NSEval	0.75	0.57	0.81	0.86
RB	-0.07	-0.10	0.02	-0.05

(b) Uncertainty analysis

The automatic algorithm pySOT was ran 200 times to investigate the modelling uncertainty caused by parameter calibration. Figure 7 presents the distributions of *NSE* values estimated by the ensemble parameter sets of the merged and original rainfall forces. It is shown that streamflow simulated by the DBMA data at the Nuxia station presented higher NSEs and smaller uncertainty ranges than that simulated by the original satellite datasets, indicating that streamflow simulations driven by the merged dataset showed stronger robustness and were less affected by uncertainty of parameter calibration.

In addition to the Nuxia hydrological station, model performance on simulating streamflow at the interior hydrological stations of Yangcun, Nugesha, Gongbujiangda and Lhasa (Figure 1) were evaluated in Figure 7. It shows that the IMERG forced simulations presented poor NSE outliers lower than zero at the Lhasa station, in spite of their good performance at the Yangcun and Nugesha stations; the GSMaP forced simulations presented large uncertainty ranges in calibration period at Nugesha and Lhasa, and in validation period at Nuxia and Gongbujiangda; the CMORPH forced simulations showed the worst performance in validation period at the interior hydrological stations, despite their sound good performance in calibration period at Yangcun and Nugesha. In comparison to the satellite datasets, the DBMA forced simulations tend to perform consistently better with smaller uncertainties at all the

hydrological stations, which can be attributed to that the merged data incorporated the advantages of different datasets in different regions and temporal periods and thus better captured the spatial variability of rainfall inputs in sub-basins.

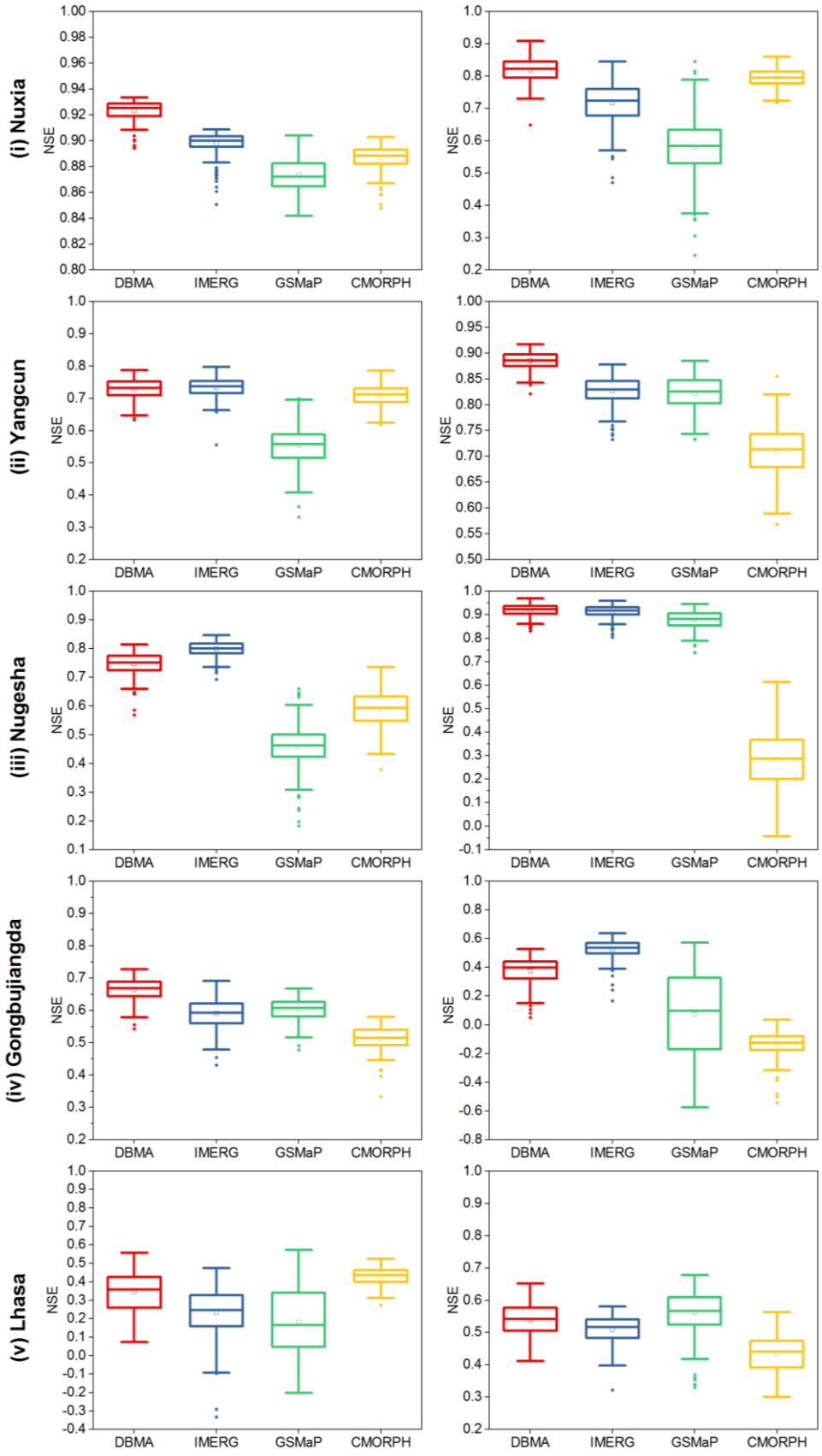

Figure 7. Runoff simulations at Nuxia, Yangcun, Nugesha, Gongbujiangda and Lhasa stations forced by multiple rainfall inputs.

4.4. Comparisons with other datasets

To avoid interference of ground gauge data that merged in the DBMA dataset, the ETC method introduced in Section 3.2 was applied to compare the three merged datasets in Table 6. The RMSE and CC of DBMA calculated by ETC were 1.11 and 0.80, respectively, both of which are obviously superior compared to the corresponding values estimated by CHIRPS and MSWEP, indicating that DBMA data is closer to the true value of rainfall in the study region.

Table 6. Statistical RMSE and CC of merged datasets calculated by the ETC method.

Datasets	DBMA	CHIRPS	MSWEP
RMSE-ETC	1.11	7.15	2.82
CC-ETC	0.80	0.28	0.62

Runoff simulations forced by the three merged datasets during June 10th 2014 to October 31st 2019 estimated by the corresponding optimal parameter sets were presented in Figure 8. Note that the daily runoff is normalized as Eq. 8 for data security reasons. Simulation by the CHIRPS data presented the lowest performance with NSE values of 0.75 and 0.78 in the calibration and validation periods, respectively. The DBMA forced simulation showed the highest performance with NSE values of 0.93 and 0.86 in the calibration and validation periods, followed by the MSWEP forced simulation which estimated NSE values of 0.9 in the calibration period and 0.76 in the validation period. The performance of streamflow forced by the merged datasets are consistent with the agreements between the merged rainfall estimates and ground truth shown in Table 6.

$$Q^n_{Normalized} = \frac{Q^n_{sim} - \min(Q_{obs})}{\max(Q_{obs}) - min(Q_{obs})} \quad (8)$$

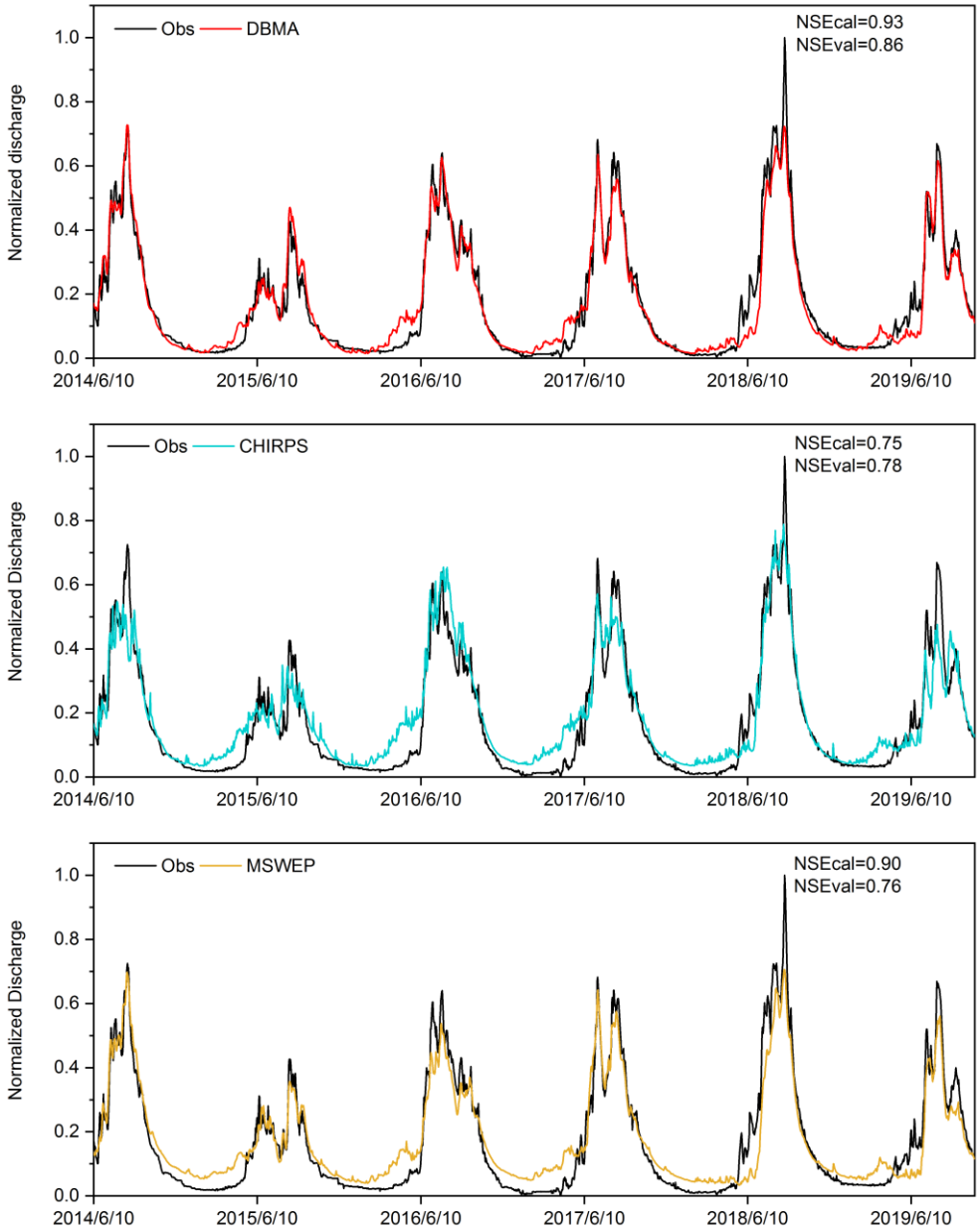

Figure 8. Simulated daily runoff at Nuxia station forced by DBMA, CHIRPS, and MSWEP.

5 Data Availability

The high-accuracy rain dataset by merging multi-satellite and dense ground gauges over southern Tibetan Plateau for the warm seasons in 2014-2019 is freely accessible at the National Tibetan Plateau Data Center https://doi.org/10.11888/Hydro.tpdc.271303 (Li et al.,2021).

6. Summary

We collated ground-based rainfall observations from a dense gauge network over southern TP. The gauged data provides crucial ground references of measured rainfall. Based on this rain gauge network and three satellite rainfall datasets of IMERG, GSMaP, and CMORPH, a merged rainfall dataset in six warm seasons from June 10th to October 31st during 2014-2019 over the southern TP was established. The DBMA method was used to estimate weights varying in space and time of the three satellite datasets for the merged data. The merged rainfall dataset presented improved performance on representing the total amount of rainfall and detecting the occurrence of gauged rainfall events, and provide a more reliable forcing for hydrological simulations in the YZRB, compared to the original satellite datasets. Comparisons with previous merged rainfall datasets of CHIRPS v2.0 and MSWEP v2 that used relatively sparse rain gauges in the study area demonstrated high values of the newly installed rain gauges for providing robust ground reference for the merging of current satellite datasets. Our results indicated that the merged datasets can meet the critical needs of accurate forcing inputs for the simulations of warm season floods and the robustness calibration of hydrological models. Based on this high-accuracy rainfall data and reliable hydrological modelling, much further research in this region then could be conducted, for example, fluvial sediment transport modelling through coupling sediment and hydrology, validation and correction of precipitation from Global Climate Model, and future runoff projections based on reliable modelling calibration in history.

Author contribution

TF and LK designed the research. LK, XR, MY developed the approach and datasets. LK downloaded the datasets and performed most of the computation and analysis work. YL, HZ, LH and MY contributed to the revising of the paper.

Competing interests

The authors declare that they have no conflict of interest.

Acknowledgements

Ground gauge data from the hydrological bureau of MWR is acknowledged here.

Financial support

This research has been financially supported by the National Natural Science Foundation of China (grant no. 92047301) and National Key R&D Program of China (2018YFC1508102).

References

Anagnostou, E. N., & Zhang, X.: Evaluation of Numerical Weather Model–Based Satellite Precipitation Adjustment in Tropical Mountainous Regions, Journal of Hydrometeorology, 20(3), 431-445, http://doi.org/10.1175/JHM-D-18-0008.1, 2019.

Beck, H. E., Wood, E. F., Pan, M., Fisher, C. K., Miralles, D. G., van Dijk, A. I. J. M., Adler, R. F.: MSWEP V2 Global 3-Hourly 0.1° Precipitation: Methodology and Quantitative Assessment, Bulletin of the American Meteorological Society, 100(3), 473-500, http://doi.org/10.1175/bams-d-17-0138.1, 2019.

Becker, A., Finger, P., Meyer-Christoffer, A., Rudolf, B., Schamm, K., Schneider, U., & Ziese, M.: A description of the global land-surface precipitation data products of the Global Precipitation Climatology Centre with sample applications including centennial (trend) analysis from 1901–present, Earth System Science Data, 5(1),

71-99, http://doi.org/10.5194/essd-5-71-2013, 2013.

Biskop, S., Maussion, F., Krause, P., & Fink, M.: Differences in the water-balance components of four lakes in the southern-central Tibetan Plateau, Hydrology and Earth System Sciences, 20(1), 209-225, http://doi.org/10.5194/hess-20-209-2016, 2016.

Bitew, M. M., & Gebremichael, M.: Evaluation through independent measurements: Complex terrain and humid tropical region in Ethiopia, Satellite rainfall applications for surface hydrology (pp. 205-214), Springer, Dordrecht, http://doi.org/ 10.1007/978-90-481-2915-7_12, 2010.

Bookhagen, B., & Burbank, D. W.: Topography, relief, and TRMM-derived rainfall variations along the Himalaya, Geophysical Research Letters, 33(8), http://doi.org/10.1029/2006gl026037, 2006.

David Eriksson, David Bindel, Christine A. Shoemaker.: pySOT and POAP: An event-driven asynchronous framework for surrogate optimization. *arXiv* preprint arXiv:1908.00420, 2019.

Derin, Y., Anagnostou, E., Anagnostou, M. N., Kalogiros, J., Casella, D., Marra, A. C., Sano, P.: Passive Microwave Rainfall Error Analysis Using High-Resolution X-Band Dual-Polarization Radar Observations in Complex Terrain, IEEE Transactions on Geoscience and Remote Sensing, 56(5), 2565-2586, http://doi.org/10.1109/tgrs.2017.2763622, 2018.

Derin, Y., Anagnostou, E., Berne, A., Borga, M., Boudevillain, B., Buytaert, W., Yilmaz, K.: Evaluation of GPM-era Global Satellite Precipitation Products over Multiple Complex Terrain Regions, Remote Sensing, 11(24), http://doi.org/10.3390/rs11242936, 2019.

Dinku, T. C., Stephen J.; Ceccato, Pietro.: Comparison of CMORPH and TRMM-3B42 over mountainous regions of Africa and South America, Satellite rainfall applications for surface hydrology (pp. 193-204): Springer, Dordrecht, http://doi.org/ 10.1007/978-90-481-2915-7_11, 2010.

449 Funk, C., Peterson, P., Landsfeld, M., Pedreros, D., Verdin, J., Shukla, S., Michaelsen,
450 J.: The climate hazards infrared precipitation with stations--a new environmental
451 record for monitoring extremes, Scientific Data, 2, 150066,
452 http://doi.org/10.1038/sdata.2015.66, 2015.
453 Gao, Y. C., & Liu, M. F.: Evaluation of high-resolution satellite precipitation products
454 using rain gauge observations over the Tibetan Plateau, Hydrology and Earth
455 System Sciences, 17(2), 837-849, http://doi.org/10.5194/hess-17-837-2013, 2013.
456 Goswami, D. C.: Brahmaputra River, Assam, India: Physiography, basin denudation,
457 and channel aggradation, Water Resources Research, 21(7), 959-978,
458 http://doi.org/ 10.1029/WR021i007p00959, 1985.
459 He, J., Yang, K., Tang, W., Lu, H., Qin, J., Chen, Y., & Li, X.: The first high-resolution
460 meteorological forcing dataset for land process studies over China, Scientific data,
461 7(1), 1-11, http://doi.org/ 10.1038/s41597-020-0369-y, 2020.
462 He, Z., Yang, L., Tian, F., Ni, G., Hou, A., & Lu, H.: Intercomparisons of Rainfall
463 Estimates from TRMM and GPM Multisatellite Products over the Upper Mekong
464 River Basin, Journal of Hydrometeorology, 18(2), 413-430,
465 http://doi.org/10.1175/jhm-d-16-0198.1, 2017.
466 Hong, Y., Gochis, D., Cheng, J.-t., Hsu, K.-l., & Sorooshian, S.: Evaluation of
467 PERSIANN-CCS Rainfall Measurement Using the NAME Event Rain Gauge
468 Network, Journal of Hydrometeorology, 8(3), 469-482,
469 http://doi.org/10.1175/jhm574.1, 2007.
470 Hou, A. Y., Kakar, R. K., Neeck, S., Azarbarzin, A. A., Kummerow, C. D., Kojima, M.,
471 Iguchi, T.: The Global Precipitation Measurement Mission, Bulletin of the
472 American Meteorological Society, 95(5), 701-722, http://doi.org/10.1175/bams-d-
473 13-00164.1, 2014.
474 Hou, S., Tian, F., Yang, L., Hu, H., & Hou, A.: How Does the Evaluation of the GPM
475 IMERG Rainfall Product Depend on Gauge Density and Rainfall Intensity?
476 Journal of Hydrometeorology, 19(2), 339-349, http://doi.org/10.1175/jhm-d-17-

0161.1, 2018.

Huang, J., Kang, S., Zhang, Q., Jenkins, M. G., Guo, J., Zhang, G., & Wang, K.: Spatial distribution and magnification processes of mercury in snow from high-elevation glaciers in the Tibetan Plateau, Atmospheric Environment, 46, 140-146, http://doi.org/10.1016/j.atmosenv.2011.10.008, 2012.

Immerzeel, W. W., Van Beek, L. P., & Bierkens, M. F.: Climate change will affect the Asian water towers, Science, 328(5984), 1382-1385, http://doi.org/ 10.1126/science.1183188, 2010.

Jiang, S., Ren, L., Hong, Y., Yong, B., Yang, X., Yuan, F., & Ma, M.: Comprehensive evaluation of multi-satellite precipitation products with a dense rain gauge network and optimally merging their simulated hydrological flows using the Bayesian model averaging method, Journal of Hydrology, 452-453, 213-225, http://doi.org/10.1016/j.jhydrol.2012.05.055, 2012.

Joyce, R. J., JE; Arkin, PA; Xie, PP.: CMORPH: A Method that Produces Global Precipitation Estimates from Passive Microwave and Infrared Data at High Spatial and Temporal Resolution, Journal of Hydrometeorology, 5(3), 487-503, 2004.

Kidd, C., & Levizzani, V.: Status of satellite precipitation retrievals, Hydrology and Earth System Sciences, 15(4), 1109-1116, http://doi.org/10.5194/hess-15-1109-2011, 2011.

Kumar, V., Jain, S. K., & Singh, Y.: Analysis of long-term rainfall trends in India. Hydrological Sciences Journal, 55(4), 484-496, http://doi.org/10.1080/02626667.2010.481373, 2010.

Liu, J., Shangguan, D., Liu, S., Ding, Y., Wang, S., & Wang, X.: Evaluation and comparison of CHIRPS and MSWEP daily-precipitation products in the Qinghai-Tibet Plateau during the period of 1981–2015, Atmospheric Research, 230, http://doi.org/ 10.1016/j.atmosres.2019.104634, 2019.

Lu, D., & Yong, B.: Evaluation and Hydrological Utility of the Latest GPM IMERG V5 and GSMaP V7 Precipitation Products over the Tibetan Plateau, Remote

505 Sensing, 10(12), http://doi.org/10.3390/rs10122022, 2018.
506 Ma, Y., Hong, Y., Chen, Y., Yang, Y., Tang, G., Yao, Y., Liu, R.: Performance of
507 Optimally Merged Multisatellite Precipitation Products Using the Dynamic
508 Bayesian Model Averaging Scheme Over the Tibetan Plateau, Journal of
509 Geophysical Research: Atmospheres, 123(2), 814-834,
510 http://doi.org/10.1002/2017jd026648, 2018.
511 McColl, K. A., Vogelzang, J., Konings, A. G., Entekhabi, D., Piles, M., & Stoffelen, A.:
512 Extended triple collocation: Estimating errors and correlation coefficients with
513 respect to an unknown target, Geophysical Research Letters, 41(17), 6229-6236,
514 http://doi.org/10.1002/2014gl061322, 2014.
515 Nash, J. E. and Sutcliffe, J. V.: River flow forecasting through conceptual models part
516 I – A discussion of principles, Journal of hydrology, 10, 282–290,
517 https://doi.org/10.1016/0022-1694(70)90255-6, 1970.
518 Parsons, D. B., Rasmussen, R. M., Dai, A., & Trenberth, K. E.: The Changing Character
519 of Precipitation, Bulletin of the American Meteorological Society, 84(9), 1205-
520 1218, http://doi.org/10.1175/bams-84-9-1205, 2003.
521 Ren, Z. H., Zhao, P., Zhang, Q., Zhang, Z. F., Cao, L. J., Yang, Y. R., & Chen, Z.:
522 Quality control procedures for hourly precipitation data from automatic weather
523 stations in China, Meteorol. Mon, 36(7), 123-132, 2010.
524 Roebeling, R. A., Wolters, E. L. A., Meirink, J. F., & Leijnse, H.: Triple Collocation of
525 Summer Precipitation Retrievals from SEVIRI over Europe with Gridded Rain
526 Gauge and Weather Radar Data, Journal of Hydrometeorology, 13(5), 1552-1566,
527 http://doi.org/10.1175/jhm-d-11-089.1, 2012.
528 Stoffelen, A.: Toward the true near-surface wind speed: Error modeling and calibration
529 using triple collocation, Journal of Geophysical Research: Oceans, 103(C4), 7755-
530 7766, http://doi.org/10.1029/97jc03180, 1998
531 Su, Y., Zhao, C., Wang, Y., & Ma, Z.: Spatiotemporal Variations of Precipitation in
532 China Using Surface Gauge Observations from 1961 to 2016, Atmosphere, 11(3),

http://doi.org/10.3390/atmos11030303, 2020.

Sun, R., Yuan, H., Liu, X., & Jiang, X.: Evaluation of the latest satellite–gauge precipitation products and their hydrologic applications over the Huaihe River basin, Journal of Hydrology, 536, 302-319, http://doi.org/10.1016/j.jhydrol.2016.02.054, 2016.

Tang, G., Ma, Y., Long, D., Zhong, L., & Hong, Y.: Evaluation of GPM Day-1 IMERG and TMPA Version-7 legacy products over Mainland China at multiple spatiotemporal scales, Journal of Hydrology, 533, 152-167, http://doi.org/10.1016/j.jhydrol.2015.12.008, 2016.

Tang, G., Clark, M. P., Papalexiou, S. M., Ma, Z., & Hong, Y.: Have satellite precipitation products improved over last two decades? A comprehensive comparison of GPM IMERG with nine satellite and reanalysis datasets, Remote Sensing of Environment, 240, http://doi.org/10.1016/j.rse.2020.111697, 2020.

Tong, K., Su, F., Yang, D., & Hao, Z.: Evaluation of satellite precipitation retrievals and their potential utilities in hydrologic modeling over the Tibetan Plateau, Journal of Hydrology, 519, 423-437, http://doi.org/10.1016/j.jhydrol.2014.07.044, 2014.

Tian, F., Hu, H., Lei, Z., & Sivapalan, M.: Extension of the Representative Elementary Watershed approach for cold regions via explicit treatment of energy related processes, Hydrology and Earth System Sciences, 10(5), 619-644, http://doi.org/10.5194/hess-10-619-2006, 2006.

Ushio, T., Sasashige, K., Kubota, T., Shige, S., Okamoto, K. i., Aonashi, K., Kawasaki, Z.-I.: A Kalman Filter Approach to the Global Satellite Mapping of Precipitation (GSMaP) from Combined Passive Microwave and Infrared Radiometric Data, Journal of the Meteorological Society of Japan, 87A, 137-151, http://doi.org/10.2151/jmsj.87A.137, 2009.

Wang, Y., Wang, L., Li, X., Zhou, J., & Hu, Z.: An integration of gauge, satellite, and reanalysis precipitation datasets for the largest river basin of the Tibetan Plateau. Earth System Science Data, 12(3), 1789-1803, http://doi.org/10.5194/essd-12-

1789-2020, 2020.

Wang, Z., Zhong, R., Lai, C., & Chen, J.: Evaluation of the GPM IMERG satellite-based precipitation products and the hydrological utility, Atmospheric Research, 196, 151-163, http://doi.org/10.1016/j.atmosres.2017.06.020, 2017.

Wilks, D. S.: Statistical methods in the atmospheric sciences (Vol. 100). Academic press, 2011.

Wolff, D. B., Nelkin, E. J., Bolvin, D. T., Huffman, G. J., Adler, R. F., Gu, G., Stocker, E. F.: The TRMM Multisatellite Precipitation Analysis (TMPA): Quasi-Global, Multiyear, Combined-Sensor Precipitation Estimates at Fine Scales, Journal of Hydrometeorology, 8(1), 38-55, http://doi.org/10.1175/jhm560.1, 2007.

Xu, R., Tian, F., Yang, L., Hu, H., Lu, H., & Hou, A.: Ground validation of GPM IMERG and TRMM 3B42V7 rainfall products over southern Tibetan Plateau based on a high-density rain gauge network, Journal of Geophysical Research: Atmospheres, 122(2), 910-924, http://doi.org/10.1002/2016jd025418, 2017.

Xue, X., Hong, Y., Limaye, A. S., Gourley, J. J., Huffman, G. J., Khan, S. I., Chen, S.: Statistical and hydrological evaluation of TRMM-based Multi-satellite Precipitation Analysis over the Wangchu Basin of Bhutan: Are the latest satellite precipitation products 3B42V7 ready for use in ungauged basins? Journal of Hydrology, 499, 91-99, http://doi.org/10.1016/j.jhydrol.2013.06.042, 2013.

Yang, D., Li, Z., Gao, B., Jiao, Y., Hong, Y., & Xu, T.: Multiscale Hydrologic Applications of the Latest Satellite Precipitation Products in the Yangtze River Basin using a Distributed Hydrologic Model, Journal of Hydrometeorology, 16(1), 407-426, http://doi.org/10.1175/jhm-d-14-0105.1, 2015

Yang, S., Chen, M., Xie, P., Yatagai, A., Hayasaka, T., Fukushima, Y., & Liu, C.: A Gauge-Based Analysis of Daily Precipitation over East Asia, Journal of Hydrometeorology, 8(3), 607-626, http://doi.org/10.1175/jhm583.1, 2007.

Yao, T., Thompson, L. G., Mosbrugger, V., Zhang, F., Ma, Y., Luo, T., & Fayziev, R.: Third pole environment (TPE). Environmental Development, 3, 52-64, 2012

589 Yilmaz, K. K., Vergara, H. J., Rodríguez-Sánchez, J.-P., Salerno, F., Sahlu, D.,
590 Nikolopoulos, E. I., Derin, Y.: Multiregional Satellite Precipitation Products
591 Evaluation over Complex Terrain, Journal of Hydrometeorology, 17(6), 1817-
592 1836, http://doi.org/10.1175/jhm-d-15-0197.1, 2016.
593 Yong, B., Chen, B., Gourley, J. J., Ren, L., Hong, Y., Chen, X., Gong, L.:
594 Intercomparison of the Version-6 and Version-7 TMPA precipitation products over
595 high and low latitudes basins with independent gauge networks: Is the newer
596 version better in both real-time and post-real-time analysis for water resources and
597 hydrologic extremes? Journal of Hydrology, 508, 77-87,
598 http://doi.org/10.1016/j.jhydrol.2013.10.050, 2014.
599 Yong, B., Hong, Y., Ren, L.-L., Gourley, J. J., Huffman, G. J., Chen, X., Khan, S. I.:
600 Assessment of evolving TRMM-based multisatellite real-time precipitation
601 estimation methods and their impacts on hydrologic prediction in a high latitude
602 basin, Journal of Geophysical Research: Atmospheres, 117(D9),
603 http://doi.org/10.1029/2011jd017069, 2012.
604 Zhai, P., Zhang, X., Wan, H., & Pan, X.: Trends in total precipitation and frequency of
605 daily precipitation extremes over China. Journal of climate, 18(7), 1096-1108,
606 http://doi.org/ 10.1175/JCLI-3318.1, 2005.
607 Zhao, Y., Zhu, J., & Xu, Y.: Establishment and assessment of the grid precipitation
608 datasets in China for recent 50 years, J. Meteor. Sci, 34(4), 414-420, 2014.